Advances in Science and Technology Research Journal

Advances in Science and Technology Research Journal 2024, 18(1), 231–243
https://doi.org/10.12913/22998624/177399
ISSN 2299-8624, License CC-BY 4.0

Received: 2023.11.22
Accepted: 2023.12.20
Published: 2024.01.15

Prediction of Buckling Behaviour of Composite Plate Element Using Artificial Neural Networks

Katarzyna Falkowicz[1*], Monika Kulisz[2]

[1] Faculty of Mechanical Engineering, Department of Machine Design and Mechatronics, Lublin University of Technology, Nadbystrzycka 36, 20-618 Lublin, Poland

[2] Faculty of Management, Department of Organisation of Enterprise, Lublin University of Technology, Nadbystrzycka 38, 20-618 Lublin, Poland

* Corresponding author's e-mail: k.falkowicz@pollub.pl

ABSTRACT

This article presents the use of artificial neural networks (ANNs) to analysis of the composite plate elements with cut-outs which can work as a spring element. The analysis were based on results from numerical approach. ANNs models have been developed utilizing the obtained numerical data to predict the composite plate's flexural-torsional form of buckling as natural form for different cut-outs and angels configurations. The ANNs models were trained and tested using a large dataset, and their accuracy is evaluated using various statistical measures. The developed ANNs models demonstrated high accuracy in predicting the critical force and buckling form of thin-walled plates with different cut-out and fiber angels configurations under compression. The combination of numerical analyses with ANNs models provides a practical and efficient solution for evaluating the stability behaviour of composite plates with cut-outs, which can be useful for design optimization and structural monitoring in engineering applications.

Keywords: artificial neural network, numerical analysis, thin-walled structures, buckling.

INTRODUCTION

Artificial intelligence (AI), with its subsets machine learning (ML) [1] and deep learning artificial neural networks (ANNs) [2–4], has recently garnered substantial attention in scientific literature [5, 6]. The evolution of ML models has been particularly noteworthy in various engineering disciplines, driven by an abundance of digital data, increasing computational capabilities, and advancements in algorithmic methodologies. Notably, ANNs have emerged as a preeminent model within the ML spectrum, also in the area of polymer composites.

The fundamental design of ANNs is profoundly influenced by the biological neural systems, enabling these networks to address complex and multifaceted challenges in both scientific and engineering domains. ANNs are adept at learning from empirical examples, which allows them to effectively navigate and interpret complex, nonlinear, and multidimensional functional relationships. This capability is pivotal, especially since it operates without the reliance on predetermined theoretical assumptions. The networks are adept at self-organizing, formulating their structure directly from the data derived from experimental observations.

Although the literature pertaining to the utilization of ANNs within the context of polymer composites is not extensive, the available studies have spanned a range of topics. These include a.o. the prediction of material fatigue, the simulation of wear patterns, the monitoring of manufacturing processes, and the intricate analysis involved in the curing of composite materials. The ability of ANNs to adapt and learn from data makes them particularly suited for these applications, where

traditional models might struggle with the complexity and variability inherent in these processes.

Moreover, the integration of ANNs in the field of polymer composites represents a significant stride towards more nuanced and data-driven approaches in material science. The potential for ANNs to contribute to breakthroughs in this field is considerable, given their ability to uncover patterns and relationships within large datasets that might otherwise remain obscured. As research continues to expand in this area, it is anticipated that the application of ANNs will become more pervasive, unlocking new possibilities and enhancing our understanding of polymer composites.

The effectiveness of ANNs models in estimating the mechanical attributes and strengths of composite materials has been presented in some papers. In their pivotal work, Zhang and Friedrich [7] introduced ANNs models designed for the assessment of fatigue life and wear characteristics of polymer composites. Additionally, ANNs have demonstrated remarkable accuracy in predicting further properties of materials, such as heat transfer coefficients and the velocity of crack propagation [8].

The Bayesian probabilistic neural network (BPNN) has been employed effectively to identify the damage type, location and extend in sandwich composite material [9]. The ANNs training algorithms success depends on the training data set and network structure [10].

In paper [11] authors used the ANN to prediction of FRP confned compressive strength of concrete and the results shows very good agreement. Similarly, in a recent study [12], an ANNs was effectively utilized to predict the compressive strength of environmentally friendly concrete containing recycled concrete aggregate, showcasing the versatility and effectiveness of ANNss models in various construction material applications. ANNs model has been also used by Malik et al. [13] to predict low velocity impact against composite plates. In paper [14] ANNs models were developed utilizing the obtained experimental and numerical data to predict the sandwich plate's natural frequencies and modal loss factors for different cut-outs configurations.

This study addresses the original concept of a thin-walled plate element with a cut-out, which can work as spring or a load-bearing element. It can be obtained by asymmetrical configuration of composite and by suitably shaped the geometric parameters of a thin-walled plate element with cut-out, without a change in its overall dimensions. More information about this conception presented in papers [15–17].

Thin-walled structural elements, can work after loss of stability if they stay within their elastic range [18–20], what poses a considerable challenge for traditional structural materials like metals, which post-critical behaviour largely hinges on their material yield strength. A key feature of these fibrous composite structures is their substantial structural load-bearing capacity, often withstanding loads up to two or three times their critical values [21–23]. Extensive research has been conducted on the performance of thin-walled laminated structures both before and after reaching critical states [24–26]. The significant load-bearing margin in composite materials enhances structural safety, as these structures preserve their rigidity till the failure load is reached, even post initial failure indicators [27–29]. The unique properties of fibrous composites, coupled with their material lightness, render them suitable for various sectors, including aviation, building [30], automotive, and aerospace industries [31], where designs frequently rely on plate and thin shell elements.

While manufacturing uniform thin plates is cost-effective, their limited bending stiffness restricts their load-bearing capacity [32, 33]. The onset of stability loss in these plates, primarily through bending, can lead to rapid failure, characterized by significant deflection with only a minor increase in compressive load, indicating low structural rigidity. However, when plates operate under a higher flexural-torsional buckling form, there's a marked improvement in their stiffness, enabling them to withstand greater compressive loads in the post-critical state.

Previous research [34, 35] has demonstrated that plates designed to undergo higher buckling forms exhibit stable and progressive post-critical equilibrium paths, making them suitable as elastic components. The behavior of such components can be tailored extensively by altering geometric parameters like the dimensions of cut-outs [36, 37] and the orientation of fibers [38, 39].

This paper introduces a straightforward approach to estimate buckling forms and buckling load in plates element under compression. These estimations were conducted using artificial neural network with using Abaqus software, a tool prevalent across diverse scientific domains [40–43].

The obtained results compared with results from previous paper [44] where Authors used analytical method to predict the form of buckling.

This paper shows the possibility of use of mathematical tool potential like ANNs in polymer composites research. The novelty is the use of the artificial neural network to predict the buckling form of compressed plate composite elements which can work as elastic elements. The cited papers and presented results in current paper shows that by good trained neural networks, and the ANNs technique we can predict the properties of material or behaviour of structure which means significant time and cost savings in both research and production. This confirm the potential of using forecasting methods in the field of mechanical engineering.

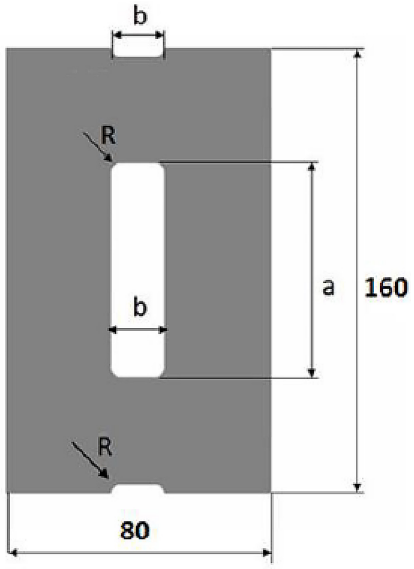

Fig. 1. Geometric parameters of tested plate element

RESEARCH SUBJECT

The investigation focused on a rectangular carbon-epoxy composite plate measuring 160x80 millimeters, featuring a central cut-out with adjustable geometric dimensions (axb) and a fillet radius (R) of 5 millimeters at the corners (Figure 1).

The composite material of the plate was characterized by anisotropic mechanical properties: a longitudinal Young's modulus (E_1) of 130.71 GPa, a transverse Young's modulus (E_2) of 6.36 GPa, a Poisson's ratio (ν_{12}) of 0.32, a shear modulus (G_{12}) of 4.18 GPa, and each layer was 0.131 millimeters thick. The plate's laminate structure was arranged in a non-symmetrical sequence of layers with the following orientation: $[0_3/\theta/-\theta/0/-\theta/\theta/-\theta/\theta/-\theta/\theta/90/\theta/-\theta/90_3]_T$, where θ represents the fiber orientation angle. More information about the model and methodology of selection the composite layout can be read in the articles [34, 35, 45].

In order to determine the critical force and the corresponding buckling form, a linear analysis was performed using FEM in the Abaqus program. Calculations were performed for various geometric parameters of the cut-out and various angles fiber orientation. The height of the cut-out was in the range of 80-120 mm and was changed every 20 mm, the width of the cut-out was in the range of 20-40 mm and was changed every 10 mm, and the angle of fiber arrangement was in the range of 15-90° and changed every 15 degrees. The data were selected deliberately as in the article [44] to be able to compare the results obtained using two different methods. Table 1 presents some part of exemplary obtained results of critical load and corresponding buckling form.

Table 1. The results of the numerical analysis for the critical state [44]

a	b [mm]	Θ [°]	Critical load [N]	Buckling form
100	20	15	1909.4	Flexural-torsional
100	20	30	1660.5	Flexural-torsional
100	20	45	1378.1	Flexural
100	20	60	1129.3	Flexural
100	20	75	1021	Flexural
100	20	90	999.6	Flexural
100	30	15	1477.2	Flexural-torsional
100	30	30	1244.4	Flexural-torsional
…	…	…	…	…
100	40	15	1151.1	Flexural-torsional
…	…	…	…	
80	30	15	1524.4	Flexural-torsional
…	…	…	…	
120	30	90	523.86	Flexural-torsional

METHODOLOGY

The Neural Net Fitting library from the MATLAB software suite was used to conduct research on artificial ANNs modeling. Two different models were developed during the study. The first model was for predicting critical force values – referred to as Model I, while the second was a classification model designed to identify the first buckling form - referred to as Model II. In the latter, the output is binary, yielding a value of 1 for flexural-torsional buckling forms and 0 for flexural buckling forms. For both models, the input layer was configured with three neurons representing the height of the cut-out (a), the width of the cut-out (b), and the angle of fiber arrangement (θ). During the training process, a shallow neural network architecture was used for both scenarios. Model I incorporated a two-layer feedforward network with sigmoid activation functions in the hidden layer and linear activation in the output neurons, an architecture conducive to regression problems. The Levenberg-Marquardt algorithm was selected as the primary learning algorithm for the network. These networks contained a single hidden layer. Through experimental methods, the optimal number of neurons within this hidden layer was determined to be in the range of 2 to 15. The architecture of the neural network for Model I is shown in Figure 2.

In the process of models evaluation, an array of 20 distinct parameter sets was utilized. This array was distributed between a principal training subset (constituting 80% of the data) and a validation subset (comprising the final 20%). The absence of a separate test dataset was a result of the limited amount of model data. In the training of ANNs, especially when confronted with a limited amount of data, it is often necessary to utilize the available data as efficiently as possible. Omitting a separate test dataset can be justified by the need to maximize the data used for training, allowing the ANNs to learn the intricacies of the data more fully. Given that an ANNs performance hinges on the volume and variety of data it is exposed to, this strategy can be crucial for developing a model that generalizes well to new data. To ensure the model's robustness in such a scenario, a validation set is indispensable. It functions as a check against overfitting, enabling the fine-tuning of the model while using the full breadth of data for training.

The evaluation of the regression model's efficiency involved a range of essential statistical measures commonly employed by researchers, as outlined in [46]. These measures are delineated below:

- Coefficient of determination (R^2):

R^2 quantifies the fraction of the variance in the dependent variable that is predictable from the independent variable(s), thereby indicating the model's explanatory power:

$$R^2 = 1 - \frac{\sum_{i=1}^{n}(y_i - y_i^{'})^2}{\sum_{i=1}^{n}(y_i - \bar{y})^2} \tag{1}$$

where: n – the number of dataset;
y_i – the real value;
y'_i – the predicted value.

- Correlation coefficient (R):

The correlation coefficient measures the intensity and polarity of a linear relationship between the actual and predicted values:

$$R(y^{'}, y^{*}) = \frac{cov(y, y^{'})}{\sigma_{y^{'}}\sigma_{y}} \quad R\epsilon < 0{,}1 > \tag{2}$$

where: σ_y – standard deviation of real data;
$\sigma_{y'}$ – standard deviation of predicted data.

- Mean squared error (MSE):

This indicator assesses the average squared variance between actual and forecasted figures, giving greater weight to more substantial discrepancies. It is defined mathematically as:

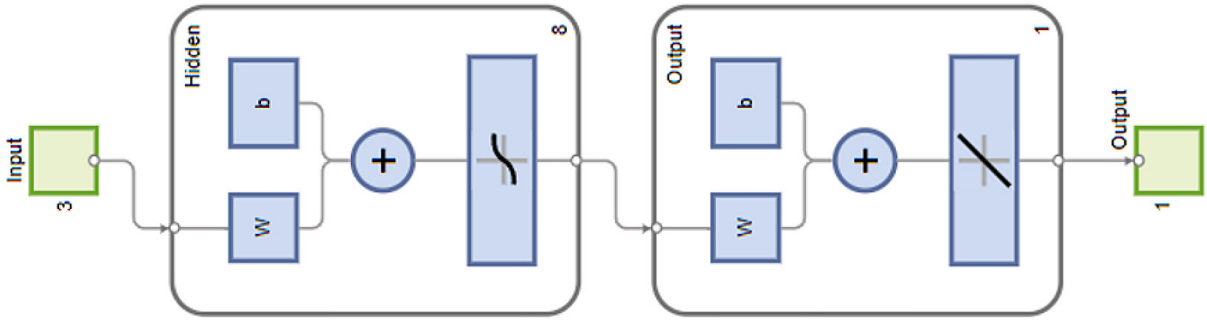

Fig. 2. The neural network architecture for Model I

$$MSE = \frac{1}{n}\sum_{i=1}^{n}(y_i - y_i^{'})^2 \quad (3)$$

- Root mean square error (RMSE):

RMSE quantifies the standard deviation of the residuals, facilitating an understanding of the error dispersion. The formula is:

$$RMSE = \sqrt{\frac{1}{n}\sum_{i=1}^{n}(y_i - y_i^{'})^2} \quad (4)$$

- Mean absolute error (MAE):

MAE computes the mean of the absolute variances between actual and predicted data, treating all errors with uniform significance. It is expressed as:

$$MAE = \frac{1}{n}\sum_{i=1}^{n}(|y_i - y_i^{'}|) \quad (5)$$

- Mean absolute percentage error (MAPE):

MAPE provides insight into the average error as a percentage, offering a comparative perspective of the prediction accuracy:

$$MAPE = \frac{1}{n}\sum_{i=1}^{n}\left|\frac{y_i - y_i^{'}}{y_i}\right| x100 \quad (6)$$

In the case of the second artificial neural network model two-layer feedforward network with sigmoid hidden neurons in the hidden layer and soft max output neurons, suitable for classification tasks, was used. The scaled conjugate gradient algorithm was used in the training process. Figure 3 shows the neural network architecture for Model II.

To evaluate the quality of classification models, three key performance indicators were employed: accuracy, confusion matrix, and ROC curve. These metrics were selected due to their broad acceptance and informative value in depicting a classifier's performance [47].

Accuracy is the simplest metric, representing the proportion of correctly classified instances out of the total instances. It is formulated as:

$$Accuracy = \frac{Number\ of\ correct\ predictions}{Total\ number\ of\ predictions} \quad (7)$$

While accuracy is straightforward and intuitive, it can be misleading in the presence of class imbalance, hence the necessity of complementary metrics [48, 49].

The confusion matrix is a tabular representation of a classifier's performance, divided into four parts: true positives (TP), true negatives (TN), false positives (FP), and false negatives (FN). It provides a more detailed insight into the nature of both correct and incorrect classifications. The elements of the confusion matrix are:

- TP: Correctly classified positive instances.
- TN: Correctly classified negative instances.
- FP: Incorrectly classified negative instances as positive.
- FN: Incorrectly classified positive instances as negative.

The ROC curve offer a comprehensive evaluation of the model's performance across different classification thresholds [50]. The ROC curve plots the true positive rate (TPR) against the false positive rate (FPR), providing insight into the trade-off between sensitivity and specificity. The TPR and FPR are defined as:

$$\mathrm{TPR} = \frac{TP}{TP + FN} \quad (8)$$

$$\mathrm{FPR} = \frac{FP}{FP + TN} \quad (9)$$

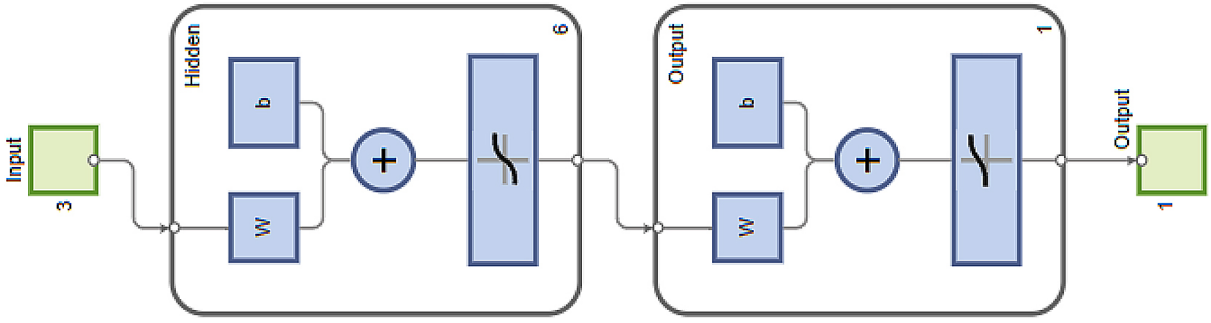

Fig. 3. The neural network architecture for Model II

RESULTS AND DISCUSSION

Modelling critical force values

Optimal modeling of the critical force parameter was achieved using a neural network architecture with eight neurons. The analysis reached its peak efficiency after running 11 epochs, as indicated in the data set. Detailed insights into the performance metrics of this neural configuration are presented in Table 2. In addition, Table 3 shows the MSE and R results for the training and validation sets, with the fifth epoch marking the point of highest validation accuracy, as shown graphically in Figure 4. The training procedure is documented in Figure 5, while Figure 6 shows the regression analyses correlating training, validation, and the data set as a whole.

Figure 7 displays a comparison of critical force values (in Newtons) for various samples (sample

Table 3. MSE and R results for the training and validation sets

Parameter	Observations	MSE	R
Training	23	156.943	0.9996
Validation	6	621.452	0.9995

Table 2. Optimal neural network training results for Model I with associated quality metrics

Training algorithm	Levenberg-Marquardt
Epoch	11
Performance	1.49
Best validation performance	621.452 at epoch 5
Gradient	43.9
Mu	1
R(all)	0.999
R^2	0.998
MSE	253.048
RMSE	15.907
MAE	12.789
MAPE	1.388

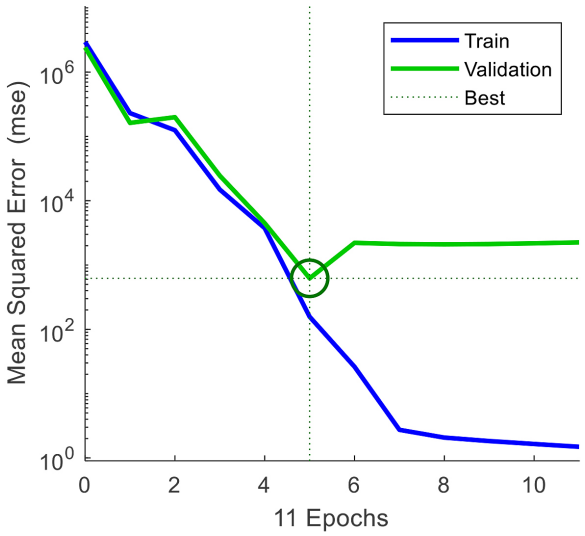

Fig. 4. Best validation performance for modelling critical force values

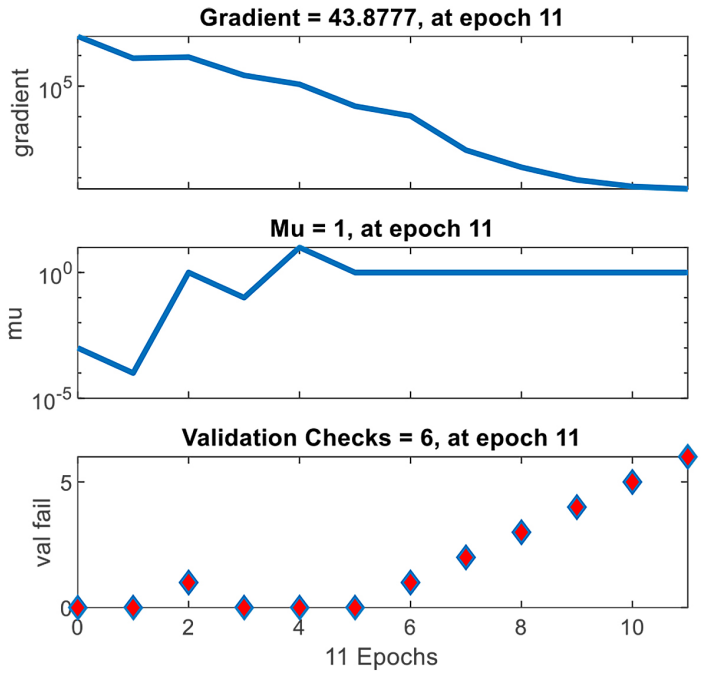

Fig. 5. Training process for modelling critical force values

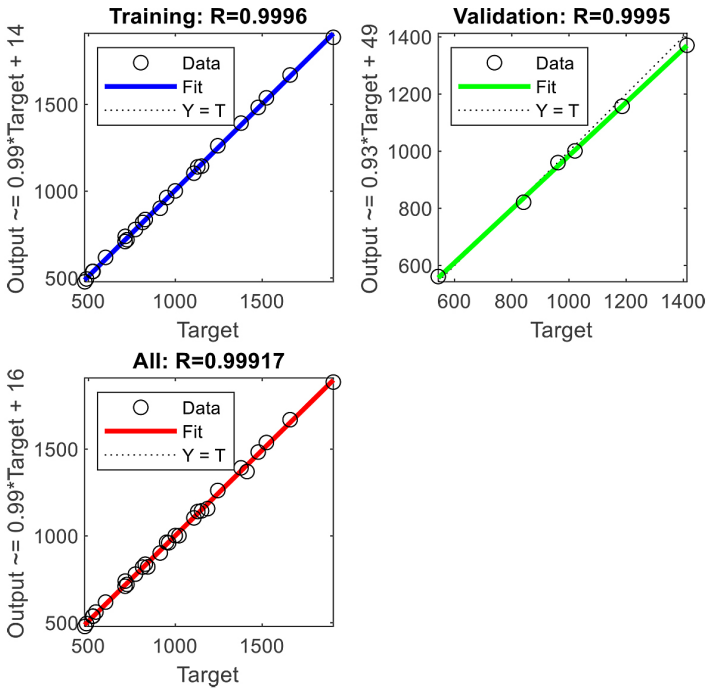

Fig. 6. ANN regression statistics for modelling critical force values

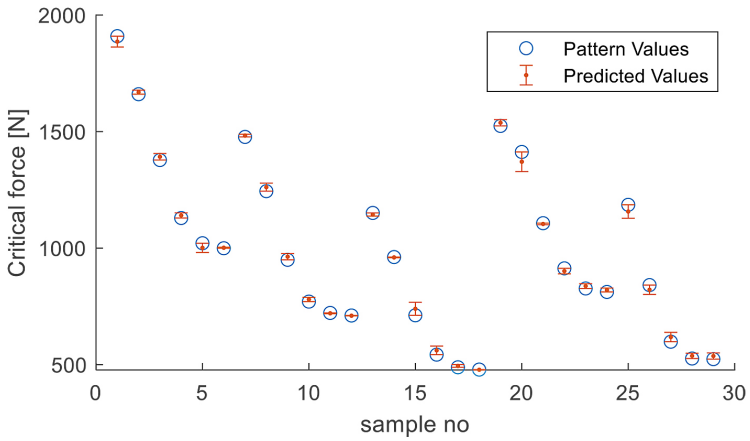

Fig. 7. Comparison of real and predicted data

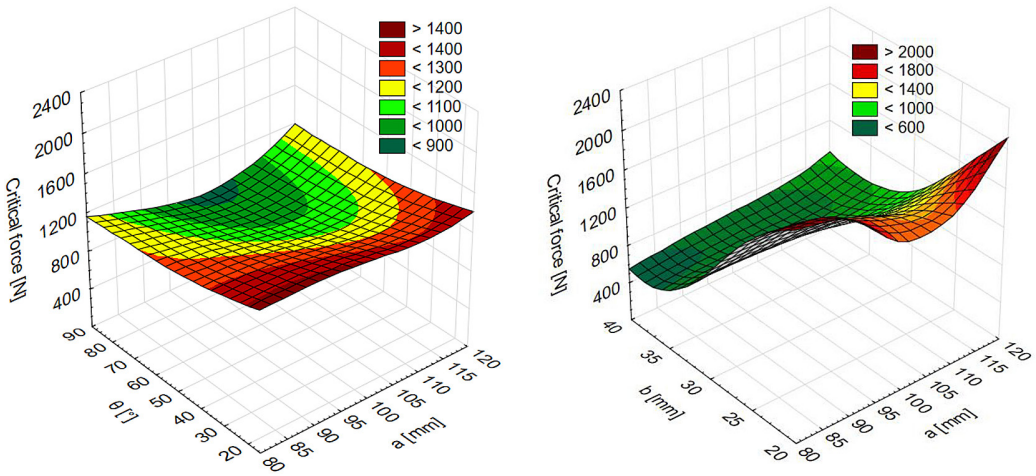

Fig. 8. Numerical results for modelling critical force values depending on the height of the cut-out a and the angle of fiber arrangement θ (a), as well as depending on the height of the cut-out a and the width of the cut-out b (b)

number on the horizontal axis). The points represent the actual measured values (labeled as "pattern values"), while the short lines with horizontal "error bars" indicate the predicted values (labeled as "predicted values"). Overall, the predicted values are close to the actual measurements with some noticeable deviation, suggesting that the forecasting model is fairly accurate.

The 3D graphs in Figure 8 show the numerical results for modelling critical force values. Due to the fact that the input to the model is 3 parameters, the model results are presented in two figures, a) on the height of the cut-out a and the angle of fiber arrangement θ and b) depending on the height of the cut-out a and the width of the cut-out b. Achieving a high level of accuracy, the model demonstrated excellent fit and predictive capability, as evidenced by the near-perfect correlation coefficients ($R > 0.999$) and low error metrics across both training and validation sets. Notably, the best validation performance was observed at the fifth epoch, suggesting an efficient training process that did not require extensive epochs to converge. These results indicate that the neural network is a robust tool for modeling critical force, with potential applications in areas where precise force prediction is critical.

Classification model identify the first buckling form

An optimized model for the classification of the identification of the first buckling was developed using an artificial neural network framework with a hexa-neuron layout. Within the collected data, peak effectiveness was observed after completion of 37 iterative training epochs. Comprehensive performance metrics for the specified neural network configuration are presented in Table 4. In addition, Table 5 presents a comparative analysis of the cross-entropy values and error metrics across the training and validation subsets. Figure 9 illustrates the decline of cross-entropy error over epochs for both the training and validation sets. It indicates that the model's validation performance improved significantly and stabilized at the 37th epoch, aligning with the results in Table 4. In addition, the receiver operating characteristic (ROC) curves, which describe the performance of the classification model, are shown in Figure 10.

Table 4. Optimal neural network training results for Model II with associated quality metrics

Training algorithm	Scaled conjugate gradient
Epoch	37
Performance	$4.13*10^{-7}$
Best validation performance	$2.681*10^{-8}$ at epoch 37
Gradient	$8.03*10^{-7}$
Accuracy	100%

Table 5. Cross-entropy and error results for the training and validation sets

Parameter	Observations	Cross-entropy	Error
Training	23	$4.133*10^{-7}$	0
Validation	6	$2.681*10^{-8}$	0

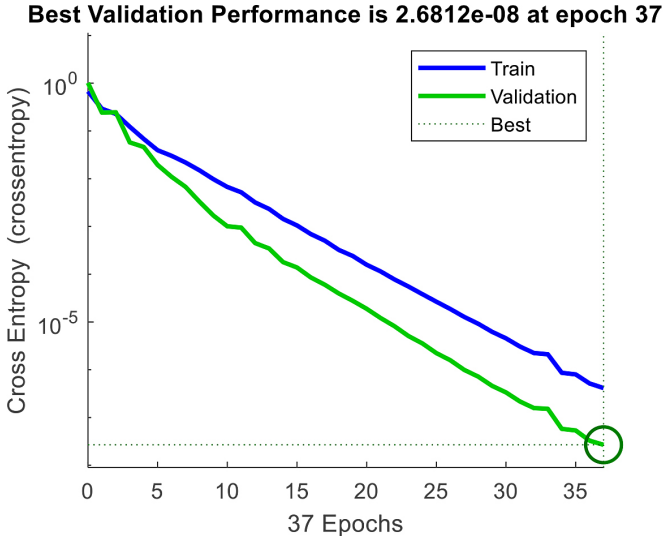

Fig. 9. Best validation performance for classification model

The ROC curves in Figure 8 display perfect classification ability with an area under the curve (AUC) of 1 for both training and validation sets, which is an indicator of an excellent model. Figure 11 presents the confusion matrices for training, validation and all data combined. The training and validation confusion matrices show that the model has achieved 100% classification accuracy, with no misclassifications observed. The test confusion matrix is not applicable (NaN%) due to a lack of test data presented. The combined matrix consolidates the overall performance, confirming the model's perfect classification accuracy on the given data. Table 6 presents exemplary results of classifier's operation.

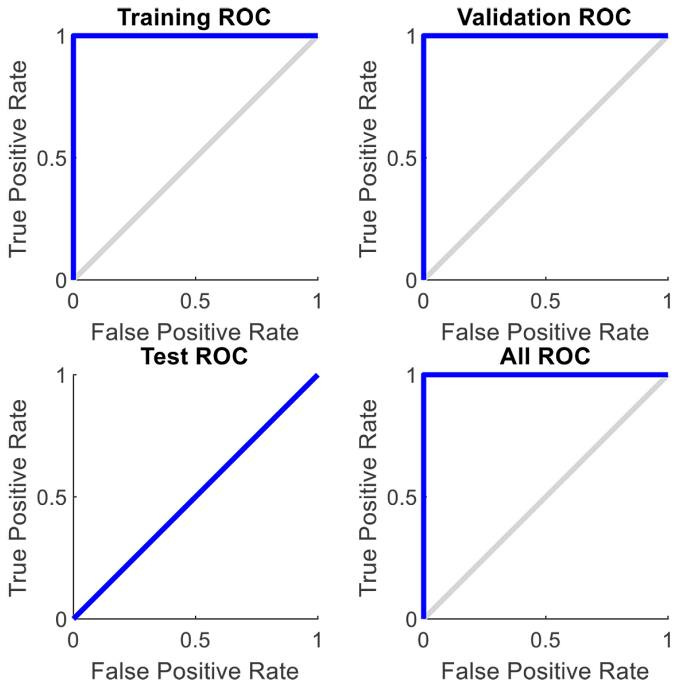

Fig. 10. Receiver operating characteristic (ROC) curves for classification model

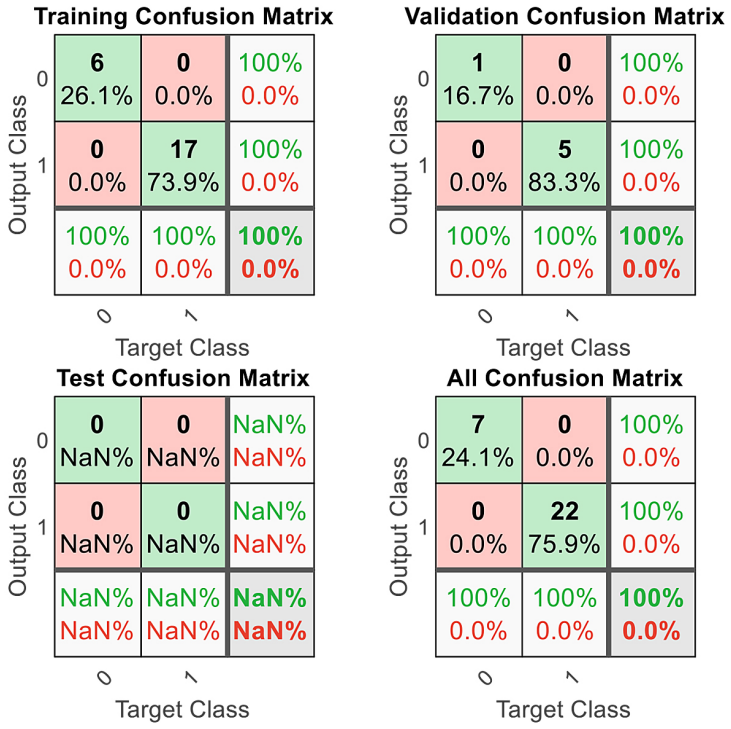

Fig. 11. Confusion matrix for classification model

Table 6. The exemplary results of classifier's operation

a [mm]	b [mm]	Θ [°]	Buckling form	Classifier's result
80	20	15	Flexural-torsional	1
80	20	20	Flexural-torsional	1
80	20	25	Flexural-torsional	1
80	20	30	Flexural	0
80	20	90	Flexural	0
90	25	15	Flexural-torsional	1
90	25	20	Flexural-torsional	1
110	30	15	Flexural-torsional	1
80	30	15	Flexural-torsional	1
120	40	15	Flexural-torsional	1
120	40	90	Flexural-torsional	1

Given the reported 100% classification accuracy of the model, it is imperative to contextualize this result within its inherent limitations and the specific conditions under which it was achieved. The high accuracy is largely due to the specialized nature of the dataset. A shallow neural network architecture was chosen which, despite its simplicity, proved to be quite effective for the specific task of buckling form classification.

In conclusion, the neural network model appears to be exceptionally well-tuned for the available data, exhibiting high accuracy and reliability in classifying the first buckling.

Moreover, the obtained results were compared with the analytical method predicting the

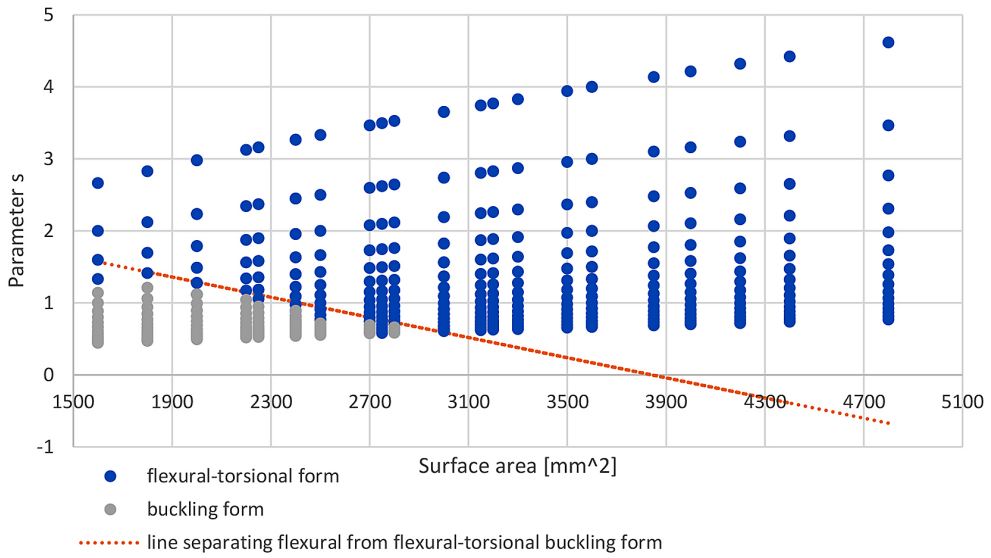

Fig. 12. Graph of buckling form depending on the area of the cut-out and parameter s (based on own study [44])

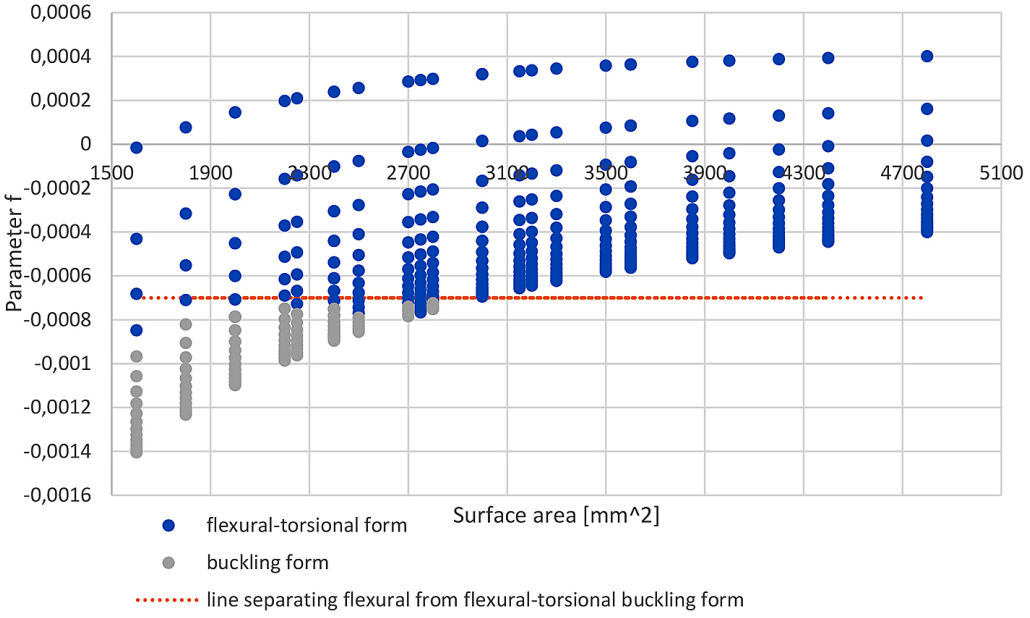

Fig. 13. Graph of buckling form depending on the area of the cut-out and parameter f (based on own study [44])

form of buckling developed in earlier work [44]. Figure 12 and 13 presents results obtained with using artificial neural networks in relation to functions designated in [44]. The developed and presented in the figures 12 and 13 function allows for separating sets on the basis of which is possible to estimate the buckling form. Results above the straight line define the flexural-torsional form, while results below the straight line define the bending form. Analyzing Figures 12 and 13, it can be seen that the results obtained using the artificial neural network refer to the approximation method used in the work [44]. Slight discrepancies can be noticed at the extreme points, but it should be emphasized that the previous method was an approximate method and it should be remember that with values close to the limit value, the results may be questionable, which was also confirmed by the obtained results presented in current paper.

CONCLUSIONS

The ANN models created showed remarkable precision in forecasting the critical force and determining the first buckling form of thin-walled plates featuring various cut-out shapes and fiber orientations under compressive forces. Integrating numerical analyses with these ANN models offers a viable and effective approach for assessing the stability characteristics of composite plates with cut-outs. This integration is potentially valuable for optimizing designs and monitoring structures in various engineering applications. The objective of the research conducted was to develop two ANNs models. The first model was designed to predict the critical force values. The second model was a classification model that identified the first buckling form. The investigation focused on a rectangular carbon-epoxy composite plate with a central cut-out with adjustable geometric dimensions.

The foundational learning algorithm selected for the model predicting critical force values was the Levenberg-Marquardt algorithm. For this model, optimal results were achieved with a network comprising eight neurons in the hidden layer. This is indicated by, among other factors, a correlation coefficient R value of 0.9996 for the training data, 0.9995 for the validation data, and 0.999 for the entire data set. In the case of the classification model, the scaled conjugate gradient algorithm was used in the learning process. This model achieved a 100% accuracy level, as evidenced by the ROC curve and an area under the curve value of 1.

The ANN models created showed remarkable precision in forecasting the critical force and determining the first buckling form of thin-walled plates featuring various cut-out shapes and fiber orientations under compressive forces. Integrating numerical analyses with these ANN models offers a viable and effective approach for assessing the stability characteristics of composite plates with cut-outs and can be expand for different type of structure. This integration is potentially valuable for optimizing designs and monitoring structures in various engineering applications.

Acknowledgments

The grant was financed in the framework of the pro-quality program of Lublin University of Technology “Grants for grants” (6/GnG/2023).

REFERENCES

1. Rogala M., Gajewski J., Górecki M. Study on the Effect of Geometrical Parameters of a Hexagonal Trigger on Energy Absorber Performance Using ANN. Materials.2021;14(20):5981.
2. Kosicka E., Krzyzak A., Dorobek M., Borowiec M. Prediction of Selected Mechanical Properties of Polymer Composites with Alumina Modifiers. Materials. 2022;15(3):882.
3. Szala M., Łatka L., Awtoniuk M., Winnicki M., Michalak M. Neural Modelling of APS Thermal Spray Process Parameters for Optimizing the Hardness, Porosity and Cavitation Erosion Resistance of Al2O3-13 wt% TiO2 Coatings. Processes. 2020;8(12):1544.
4. Singh J., Vasudev H., Szala M., Gill H.S. Neural computing for erosion assessment in Al-20TiO2 HVOF thermal spray coating. Int J Interact Des Manuf. 2023; https://link.springer.com/10.1007/s12008-023-01372-y.
5. Karpiński R., Krakowski P., Jonak J., Machrowska A., Maciejewski M., Nogalski A. Diagnostics of Articular Cartilage Damage Based on Generated Acoustic Signals Using ANN—Part I: Femoral-Tibial Joint. Sensors. 2022;22(6):2176.
6. Machrowska A., Szabelski J., Karpiński R., Krakowski P., Jonak J., Jonak K. Use of Deep Learning Networks and Statistical Modeling to Predict Changes in Mechanical Parameters of Contaminated Bone Cements. Materials. 2020;13(23):5419.

7. Zhang Z., Friedrich K. Artificial neural networks applied to polymer composites: a review. Composites Science and Technology. 2003;63(14):2029–44.
8. Lucon P.A., Donovan R.P. An artificial neural network approach to multiphase continua constitutive modeling. Composites Part B: Engineering. 2007;38(7–8):817–23.
9. Just-Agosto F.., Serrano D, Shafiq B., Cecchini A. Neural network based nondestructive evaluation of sandwich composites. Composites Part B: Engineering. 2008;39(1):217–25.
10. Boğa A.R., Öztürk M., Topçu İ.B. Using ANN and ANFIS to predict the mechanical and chloride permeability properties of concrete containing GGBFS and CNI. Composites Part B: Engineering. 2013;45(1):688–96.
11. Naderpour H., Kheyroddin A.., Amiri GG. Prediction of FRP-confined compressive strength of concrete using artificial neural networks. Composite Structures. 2010;92(12):2817–29.
12. Kulisz M., Kujawska J.., Aubakirova Z, Zhairbaeva G., Warowny T. Prediction of The Compressive Strength Of Environmentally Friendly Concrete Using Artificial Neural Network. acs. 2022;18(4):68–81.
13. Malik M.H., Arif A.F.M. ANN prediction model for composite plates against low velocity impact loads using finite element analysis. Composite Structures. 2013;101:290–300.
14. Prusty J.K., Papazafeiropoulos G., Mohanty S.C. Free vibration analysis of sandwich plates with cutouts: An experimental and numerical study with artificial neural network modelling. Composite Structures. 2023;321:117328.
15. Falkowicz K., Debski H. The work of a compressed, composite plate in asymmetrical arrangement of layers. W Depok, Indonesia; 2019; s. 020005. http://aip.scitation.org/doi/abs/10.1063/1.5092008
16. Falkowicz K., Debski H., Wysmulski P. Effect of extension-twisting and extension-bending coupling on a compressed plate with a cut-out. Composite Structures. 2020;238:111941.
17. Falkowicz K. Composite plate analysis made in an unsymmetric configuartion. J Phys: Conf Ser. 2021;2130(1):012014.
18. Wysmulski P., Debski H., Falkowicz K. Sensitivity of Compressed Composite Channel Columns to Eccentric Loading. Materials. 2022;15(19):6938.
19. Falkowicz K. Numerical Buckling Analysis of Thin-Walled Channel-Section Composite Profiles Weakened by Cut-Outs. Adv Sci Technol Res J. 2022;16(6):88–96.
20. Wysmulski P. The effect of load eccentricity on the compressed CFRP Z-shaped columns in the weak post-critical state. Composite Structures. 2022;301:116184.
21. Banat D., Mania R. Failure analysis of thin-walled GLARE members during buckling and post-buckling response. In Zakopane, Poland; 2019; s. 020001. https://pubs.aip.org/aip/acp/article/736694.
22. Bazant Z.P., Cedolin L., Hutchinson J.W. Stability of Structures: Elastic, Inelastic, Fracture, and Damage Theories. Journal of Applied Mechanics. 1993;60(2):567–8.
23. Wysmulski P. The analysis of buckling and post buckling in the compressed composite columns. Archives of Materials Science and Engineering. 2017;85(1):35–41.
24. Różyło P., Dębski H., Kral J. Buckling and limit states of composite profiles with top-hat channel section subjected to axial compression. *AIP Conf. Proc.* 2018, 1922, 080001. https://pubs.aip.org/aip/acp/article/608612.
25. Debski H., Samborski S, Rozylo P, Wysmulski P. Stability and Load-Carrying Capacity of Thin-Walled FRP Composite Z-Profiles under Eccentric Compression. Materials. 2020;13(13):2956.
26. Debski H., Rozylo P., Wysmulski P. Stability and load-carrying capacity of short open-section composite columns under eccentric compression loading. Composite Structures. 2020;252:112716.
27. Falkowicz K. Experimental and numerical failure analysis of thin-walled composite plates using progressive failure analysis. Composite Structures. 2023;305:116474.
28. Rozylo P., Falkowicz K. Stability and failure analysis of compressed thin-walled composite structures with central cut-out, using three advanced independent damage models. Composite Structures. 2021;273:114298.
29. Banat D., Mania R.J., Degenhardt R. Stress state failure analysis of thin-walled GLARE composite members subjected to axial loading in the post-buckling range. Composite Structures. 2022;289:115468.
30. Chróścielewski J., Miśkiewicz M., Pyrzowski Ł., Rucka M., Sobczyk B., Wilde K. Modal properties identification of a novel sandwich footbridge – Comparison of measured dynamic response and FEA. Composites Part B: Engineering. 2018;151:245–55.
31. Bakunowicz J., Kopecki T., Lis T., Mazurek P. Effect of stiffeners on nature of post-critical deformations of thin-walled composite aircraft structures: A combined numerical-experimental study. W: 2016 7th International Conference on Mechanical and Aerospace Engineering (ICMAE) [Internet]. London, United Kingdom: IEEE; 2016; s. 46–53. http://ieeexplore.ieee.org/document/7549506/.
32. Singer J., Arbocz J., Weller T. Buckling experiments: experimental methods in buckling of thin-walled structures. Chichester; New York: Wiley; 1998. 2 s.

33. Koiter W.T., Heijden A.M.A. van der. W.T. Koiter's elastic stability of solids and structures. Cambridge ; New York: Cambridge University Press; 2009. 230 s.
34. Falkowicz K., Samborski S., Valvo P.S. Effects of Elastic Couplings in a Compressed Plate Element with Cut-Out. Materials. 2022;15(21):7752.
35. Falkowicz K. Validation of Extension-Bending and Extension-Twisting Coupled Laminates in Elastic Element. Adv Sci Technol Res J. 2023;17(3):309–19.
36. Falkowicz K. Buckling numerical analysis of composite plate element in asymmetrical configuration. J Phys: Conf Ser. 2021;1736(1):012029.
37. Falkowicz K., Debski H., Teter A. Design solutions for improving the lowest buckling loads of a thin laminate plate with notch. In Lublin, Poland; 2018; s. 080004. http://aip.scitation.org/doi/abs/10.1063/1.5019075.
38. Falkowicz K., Wysmulski P., Debski H. Buckling Analysis of Laminated Plates with Asymmetric Layup by Approximation Method. Materials. 2023;16(14):4948.
39. Wysmulski P., Falkowicz K., Filipek P. Buckling state analysis of compressed composite plates with cut-out. Composite Structures. 2021;274:114345.
40. Jonak J., Karpiński R., Wójcik A. Numerical analysis of the effect of embedment depth on the geometry of the cone failure. J Phys: Conf Ser. 2021;2130(1):012012.
41. Kopecki T., Święch Ł. Experimental-Numerical Analysis of a Flat Plate Subjected to Shearing and Manufactured by Incremental Techniques. Adv Sci Technol Res J. 2023;17(4):179–88.
42. Rzeczkowski J., Paśnik J., Samborski S. Corrigendum to "Mode III numerical analysis of composite laminates with elastic couplings in split cantilever beam configuration". Composite Structures. 2021;266:113920.
43. Couto R., Couto A., Arachchige D., Nascimento D., Moreira R., De Moura M., i in. Numerical analysis on the strength prediction of composite bonded repairs under different loading scenarios. Journal of Composite Materials. 2023;57(19):3025–43.
44. Falkowicz K., Szklarek K. Analytical method for projecting the buckling form of composite palates with a cut-out. IOP Conf Ser: Mater Sci Eng. 2019;710(1):012021.
45. Falkowicz K., Debski H. The post-critical behaviour of compressed plate with non-standard play orientation. Composite Structures. 2020;252:112701.
46. Kujawska J., Kulisz M., Oleszczuk P, Cel W. Machine Learning Methods to Forecast the Concentration of PM10 in Lublin, Poland. Energies. 2022;15(17):6428.
47. Kłosowski G., Kulisz M. Identification of surface defects using deep and transfer learning. J Phys: Conf Ser. 2022;2408(1):012028.
48. Karpiński R., Krakowski P., Jonak J., Machrowska A., Maciejewski M., Nogalski A. Diagnostics of Articular Cartilage Damage Based on Generated Acoustic Signals Using ANN—Part II: Patellofemoral Joint. Sensors. 2022;22(10):3765.
49. Szabelski J., Karpiński R., Machrowska A. Application of an Artificial Neural Network in the Modelling of Heat Curing Effects on the Strength of Adhesive Joints at Elevated Temperature with Imprecise Adhesive Mix Ratios. Materials. 2022;15(3):721.
50. Karpiński R. Knee Joint Osteoarthritis Diagnosis Based On Selected Acoustic Signal Discriminants Using Machine Learning. acs. 2022;18(2):71–85.